J Solid State Electrochem (2014) 18:3345–3357
DOI 10.1007/s10008-014-2622-9

ORIGINAL PAPER

Electrocatalytic and SERS activity of Pt rich Pt-Pb nanostructures formed via the utilisation of in-situ underpotential deposition of lead

Blake J. Plowman · Muhammad E. Abdelhamid · Samuel J. Ippolito · Vipul Bansal · Suresh K. Bhargava · Anthony P. O'Mullane

Received: 4 June 2014 / Revised: 21 August 2014 / Accepted: 23 August 2014 / Published online: 5 September 2014

Abstract The controlled synthesis of nanostructured materials remains an ongoing area of research, especially as the size, shape and composition of nanomaterials can greatly influence their properties and applications. In this work, we present the electrodeposition of highly dendritic platinum rich platinum-lead nanostructures, where lead acetate acts as an inorganic shape directing agent via underpotential deposition on the growing electrodeposit. It was found that these nanomaterials readily oxidise at potentials below monolayer oxide formation, which significantly impacts on the methanol electrooxidation reaction and correlates with the Incipient Hydrous Oxide Adatom Mediator (IHOAM) model of electrocatalysis. Additionally, these materials were tested for their surface enhanced Raman scattering (SERS) activity, where the high density of sharp tips provides promise for their application as SERS substrates.

Keywords Platinum-lead · Bimetallic · Nanostructures · Electrocatalysis · Electrodeposition

Electronic supplementary material The online version of this article (doi:10.1007/s10008-014-2622-9) contains supplementary material, which is available to authorized users.

B. J. Plowman · S. J. Ippolito · V. Bansal · S. K. Bhargava
Centre for Advanced Materials and Industrial Chemistry, RMIT University, GPO Box 2476V, Melbourne, VIC, Australia

B. J. Plowman · M. E. Abdelhamid · S. J. Ippolito · V. Bansal · S. K. Bhargava · A. P. O'Mullane
School of Applied Sciences, RMIT University, GPO Box 2476V, Melbourne, VIC, Australia

A. P. O'Mullane (✉)
School of Chemistry, Physics and Mechanical Engineering, Queensland University of Technology, GPO Box 2434, Brisbane, QLD 4001, Australia
e-mail: anthony.omullane@qut.edu.au

Introduction

The formation of nanostructured materials through electrochemical methods has recently received significant interest due to the ability to control important factors such as shape, size, crystallographic orientation, coverage and thickness. It has been identified that fabricating hierarchical nanostructures such as octahedra, nanoflowers and nanothorns, which consist of sharp edges, are more beneficial for catalytic and surface enhanced Raman scattering (SERS) applications compared to regularly synthesized spherical particles [1–3]. This is due, in the former application, to the high reactivity at the tips of such nanostructures that most likely consist of low lattice stabilised metal atoms [4]. In SERS applications, well-defined edges and corners facilitate the induction of a greater localised field which results in large signal enhancements [1].

Platinum is an extremely important material given its electrocatalytic and sensing properties [5–18]. The shape controlled chemical synthesis of platinum nanoparticles has been achieved to generate spheres, cubes, rods and hierarchical structures [7, 8, 13, 16, 19–22] but inherently the synthesis can be difficult. Also, homogeneous immobilisation and strong adherence to a solid support can be challenging, which is often required for many applications. The electrochemical formation of platinum nanostructures offers an alternative method to achieve shape control while ensuring good adherence to the underlying support, although the former has proved to be more difficult than chemical synthesis routes. However, some recent studies have shown that it is possible through electrochemical methods to generate Pt nanorods by deposition into titania nanopillar templates [15] or that nanostructures with exposed high-index facets can be achieved through either direct electrodeposition or by a post synthesis redox treatment of preformed seed nanoparticles [18, 23, 24]. Other approaches to generate hierarchical nanostructures have

included modifying an electrode surface prior to electrodeposition with either a polymeric layer [25–27] or including metal oxides as an assisting agent within a carbon black support [28]. The inclusion of surfactants in solution has also led to the electrochemical deposition of high surface area nanoporous platinum [29, 30]. However, in many of these approaches, either specialised templates are required or the Pt nanostructures are either chemically modified by organic surfactants or are deposited on a surface containing chemical functional groups that may interfere in a detrimental manner with the performance of the nanostructured materials for some applications. Therefore, it is desirable to achieve shape control through approaches which do not employ organic surfactants or templates. To alleviate this problem, inorganic salts such as lead acetate have been employed in the electrodeposition of Pt to form Pt black [31] and dendritic type Pt deposits [32]. However, in the latter case, there lacked a detailed explanation into the role that lead acetate plays in controlling the anisotropic growth of Pt.

Alongside these efforts to control the morphology of noble metal nanomaterials, there has been much work focussed on improving their electrocatalytic reactivity through chemical, electrochemical and thermal methods. Chemical methods have included pretreatment of gold nanoparticles with sodium borohydride to enhance their activity by insertion of hydrogen into or onto the nanoparticles [33]. Electrochemical treatments have included polarisation of gold and platinum electrodes in the hydrogen evolution region [34–42], and thermal methods involved electrical resistive heating of wire electrodes followed by rapid quenching in air or water [36, 38]. In these cases, the result is the fabrication of metal surfaces or nanoparticles rich in active states which under certain experimental conditions enhance their electrocatalytic activity [42–44]. This increase in activity, in particular for oxidation reactions, has been proposed to be due to the formation of incipient oxides on the electrode surface that may mediate electrocatalytic processes and has been described in the Incipient Hydrous Oxide Adatom Mediator (IHOAM) model of electrocatalysis [6, 35, 45]. The generation of active states which involves creating atoms or clusters of atoms with low lattice coordination numbers and therefore larger surface energy makes them prone to oxidation at potentials prior to the formation of the bulk compact oxide and is often denoted as premonolayer oxidation [41]. However, the ability to generate high surface area and active catalysts without pretreatment procedures is highly desirable which may be achievable through the direct electrodeposition of hierarchical nanostructures. With this approach, there still remains a challenge to generate nanomaterials with the optimum level of surface defects. Indeed, this is a challenge at any surface as Scholz recently demonstrated that active sites are present on a range of electrode materials and can significantly influence inner sphere electrocatalytic reactions [46, 47]. In fact, the creation of surfaces with overly active sites has also been reported to be prone to extensive oxidation which can ultimately lead to suppressed electrocatalytic activity [36, 48]. Additionally, the influence of morphology and crystallographic orientation of dispersed metal nanomaterials on the kinetics of electrocatalytic reactions is still not completely understood and requires further investigation [49].

SERS is a powerful analytical technique that has been widely studied on surfaces consisting of gold, silver and copper where the surface morphology of the substrate is highly influential on the quality of the signal. Significantly, fewer studies have reported on SERS activity of other transition metals such as Pt which will be of benefit for the study of electrocatalytic mechanisms and the fabrication of a surface for sensing applications that is not prone to significant oxidative deterioration such as silver and copper. To date, the fabrication of SERS active Pt substrates has included the use of templates to produce well-ordered surfaces, electrochemical roughening protocols, columns loaded with nanoparticles, the deposition of Pt thin films onto SERS active materials or the use of an applied potential to a nanostructured substrate to monitor SERS activity [2, 5, 50–54]. Although each of these methods produce SERS active Pt substrates, it is still desirable to explore other methods to fabricate reproducible, robust and stable nanostructured surfaces which can be achieved in a rapid and facile manner through electrochemical metal deposition.

In this work, it is shown that through the use of a simple inorganic growth directional agent such as lead acetate, $Pb(CH_3COO)_2$, that hierarchical Pt nanostructures of various sizes and shapes can be achieved. This approach involves the concurrent underpotential deposition of lead alongside the bulk electrodeposition of platinum, resulting in the formation of nanostructures which show significantly enhanced activity for electrocatalysis as well as SERS applications.

Experimental

Materials

Aqueous 1.0 M H_2SO_4 and 0.1 M HCl (Aldrich) solutions were made up with deionized water (resistivity of 18.2 MΩ cm) purified by use of a Milli-Q reagent deioniser (Millipore). H_2PtCl_6, K_2PtCl_6, $Pb(CH_3COO)_2{\cdot}3H_2O$, sodium nitrate (Aldrich), sodium acetate (Ajax), lead nitrate (BDH), Rhodamine B and methanol (Merck) were used as received.

Electrochemical measurements

Voltammetric experiments were conducted at 20±2 °C with a CH Instruments (CHI 760C) electrochemical analyzer in an electrochemical cell that allowed reproducible positioning of

the working, reference, and auxiliary electrodes and a nitrogen inlet tube. A 1.6-mm-diameter platinum electrode (BAS) and glassy carbon plates (Sigradur G, HTW) were used as working electrodes, with the geometric area of the latter defined by the addition of a polyimide tape (ATA Distributors) with an exposed circular region of 4.5 mm in diameter. Prior to electrodeposition, each electrode was polished with aqueous 0.3 μm alumina slurry on a polishing cloth (Microcloth, Buehler), thoroughly rinsed with Milli-Q water and dried with a flow of nitrogen gas. Prior to using indium tin oxide (ITO) (Delta Technologies Ltd.) coated glass with a sheet resistance of 4–8 Ω/sq (as quoted by the manufacturer) as the working electrode (area of 0.16 cm^2), each sample was sonicated in acetone and then methanol for 5 min and blown dry with a flow of nitrogen gas. The reference electrode was Ag/AgCl (aqueous 3 M KCl). For electrodeposition experiments, GC and ITO electrodes were used as the working electrode and a graphite rod (6 mm diameter, Johnson Matthey Ultra "F' purity grade) as the counter electrode to avoid any contamination from dissolution products that may occur during the electrolysis. For cyclic voltammetric studies, the counter electrode was also a graphite rod. All electrochemical experiments were commenced after degassing the electrolyte solutions with nitrogen for at least 10 min prior to any measurement.

Physical characterisation

Scanning electron microscopy (SEM) measurements were performed on a FEI Nova SEM instrument with an AMETEK energy dispersive X-ray (EDX) system (Nova 200) operated at an accelerating voltage of 30 kV. Prior to SEM imaging, samples were thoroughly rinsed with Milli-Q water and dried under a flow of nitrogen. The average particle size was determined from low magnification SEM images at ×25,000 and ×13,000 magnifications for Pt and PtPb materials, respectively, using ImageJ software where at least 300 particles were analysed. X-ray diffraction data were obtained with a Bruker AX 8: Discover with General Area Detector Diffraction System (GADDS). It should be noted that the GC substrate does give rise to broad peaks which have been background subtracted from the data obtained at the GC/Pt samples. Samples for transmission electron microscopy (TEM) were prepared by sonicating the Pt/ITO samples in methanol for 60 min and then drop cast onto a carbon coated copper grid and performed using a JEOL 1010 TEM instrument operated at an accelerating voltage of 100 kV. X-ray photoelectron spectroscopy (XPS) measurements of Pt nanomaterials electrodeposited were carried out on a Thermo K-Alpha XPS instrument at a pressure better than 1×10^{-9} Torr. The core level binding energies (BEs) were aligned to the adventitious C 1 s binding energy of 285 eV. SERS measurements were carried out with a PerkinElmer RamanStation 400 at an excitation wavelength of 785 nm. Samples were prepared by immersing the GC/Pt nanostructured substrate in a 1 mM solution of Rhodamine B for 1 h, rinsed with a copious amount of Milli-Q water and then blown dry with nitrogen.

Results and discussion

The electrodeposition of platinum was investigated using cyclic voltammetry (CV) from a solution containing 8 mM K_2PtCl_6 in 0.1 M HCl (Fig. 1a). Shown in black is the response of a glassy carbon electrode, where the reduction of the $PtCl_6^{2-}$ salt can be observed at potentials below ca. 0.27 V. In the presence of a large concentration of chloride ions, as is the case here, the formation of the Pt(II) intermediate ($PtCl_4^{2-}$) is suppressed and the direct four electron reduction to metallic platinum occurs [55]. Towards the lower limit of the scan, a small but sharp reduction process can be observed (below ca. −0.18 V), which is attributed to the evolution of hydrogen from the acidic solution at the Pt nuclei electrodeposited on the glassy carbon surface in the forward sweep. Upon reversing the scan at −0.2 V, no additional peaks can be detected, indicating that the reduction of the platinum salt is irreversible.

The electrochemical behaviour of this system was then tested after the addition of 0.05 mM $Pb(CH_3COO)_2$ (Fig. 1a, red curve). At potentials above 0 V, this displayed almost identical behaviour to the scan in the absence of lead acetate; however, below this value, the reduction continues until reaching a sharp peak at ca. -0.03 V. Noticeably, the current magnitude of this peak is increased when lead acetate is present, as is the hydrogen evolution reaction at the lower potential range. These features indicate that the rate of platinum electrodeposition is higher in the presence of lead acetate across this potential range.

In order to further study the influence of lead acetate on the electrodeposition of platinum, cyclic voltammetric experiments were conducted (Fig. 1b) in the absence of K_2PtCl_6 in a solution of 0.1 M HCl in the absence (black) or presence (red) of 0.5 mM $Pb(CH_3COO)_2$ at electrodes which were previously modified with nanostructured Pt surfaces as shown in Fig. 2b. It should be noted that the concentration of $Pb(CH_3COO)_2$ is tenfold higher than that used for the electrodeposition studies, in order to produce a significant electrochemical signal and clarify the role of the lead acetate. From these cyclic voltammograms, it can be seen that a quasi-reversible process occurs on the platinum nanostructures in the presence of lead acetate, with a reduction peak centred at 0.37 V followed by an oxidative counterpart at 0.47 V. These features are assigned to the underpotential deposition (UPD) and stripping of lead on platinum [56] in the forward and reverse scans, respectively, demonstrating that platinum

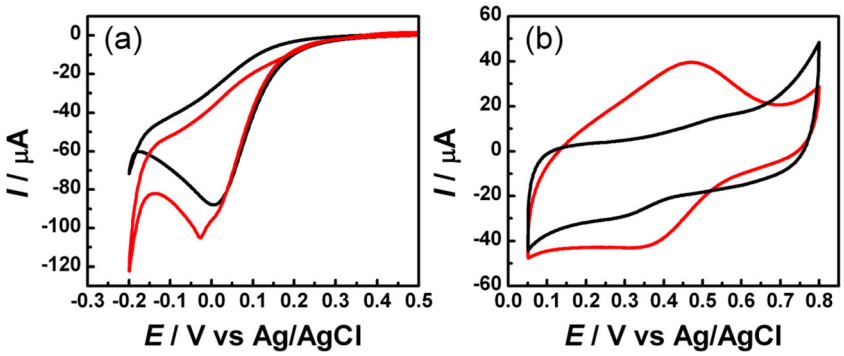

Fig. 1 **a** CVs recorded at a glassy carbon electrode in 8 mM K_2PtCl_6 in 0.1 M HCl with (red) or without (black) the addition of 0.05 mM $Pb(CH_3COO)_2$. **b** CVs of electrodeposited platinum-lead nanostructures in 0.1 M HCl in the absence (*black*) or presence (*red*) of 0.5 mM $Pb(CH_3COO)_2$. Scan rates in all cases were 50 mV s

deposition under the conditions given for Fig. 1a is accompanied by Pb UPD. This latter process is however not directly observed in Fig. 1a as the platinum nuclei required for Pb UPD are not formed on the glassy carbon surface until ca. 0.27 V. However, the UPD of lead on platinum is expected to occur under constant potential electrodeposition conditions once a potential below 0.37 V is applied.

Having observed that the presence of lead acetate influences the electroreduction of $PtCl_6^{2-}$ ions below ca. 0 V, the effect that this has on the morphology of the deposits was then examined by scanning electron microscopy (SEM) imaging. This was performed by electrodepositing at −0.05 V for 600 s, where the potential lies at a suitable value to study the perturbed electrodeposition of platinum in the presence of lead acetate while avoiding the hydrogen evolution region, which may also affect the morphology of electrodeposited materials as shown in a recent study [57]. Figure 2a shows SEM images of Pt nanoparticles electrodeposited on a glassy carbon substrate under these conditions in the absence of lead acetate. It can be seen that these particles are quasi-spherical in nature, with an average size of ca. 320 nm. Amongst these nanostructures are a number of smaller particles (ca. 180 nm in diameter) which appear to have formed through the progressive nucleation of platinum on the glassy carbon surface. While the majority of the particles are isolated, it can be seen that several particles are connected, due to the growth of two nearby nuclei until they merge into larger structures. The fine features of the particles are visible in the inset of Fig. 2a, showing a surface consisting of a slightly roughened texture on a number of small pyramid-like protrusions.

Upon the introduction of lead acetate into the deposition solution, significant changes can be observed in the morphology of the electrodeposited surfaces (Fig. 2b). Here, the growths become dendritic, with a large number of exposed tips on the surface with features appearing below 10 nm. Interestingly, these sub-10 nm features lie in a size range which has been reported to be beneficial for catalytic and electrocatalytic applications [53, 58]. The growth of these dendrite-like structures again occurs at isolated nuclei, which then grow to be larger than the quasi-spherical structures deposited in the absence of lead acetate, with typical sizes of ca. 1 μm (average size was 800 nm). It should also be noted that control electrodeposition experiments were performed in the presence of 0.05 mM sodium acetate or 0.05 mM sodium nitrate in place of lead acetate so that the influence of the anions and cations on the morphology of the electrodeposits could be determined. From these experiments, it was found that quasi-spherical deposits were formed in both cases (Fig. S1), illustrating that the dendritic growth is achieved by the inclusion of Pb^{2+} ions in the deposition solution as opposed to the effect of the acetate anions present in the solution.

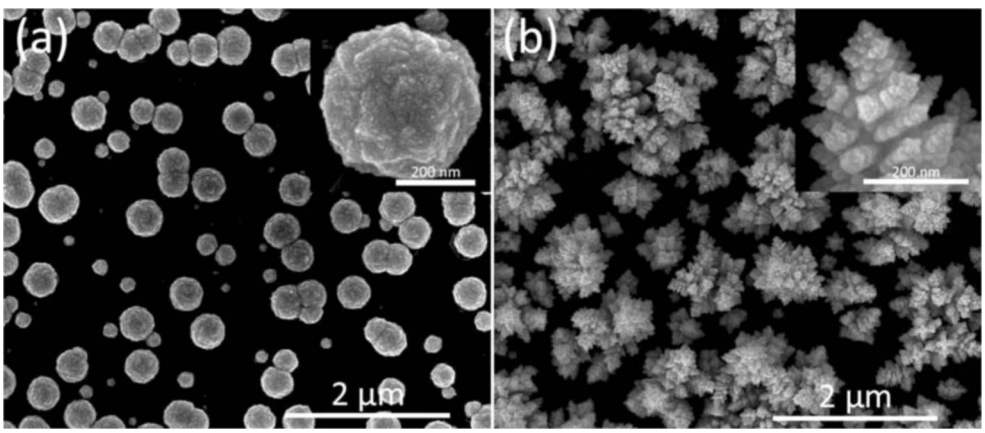

Fig. 2 SEM images of samples electrodeposited at −0.05 V for 600 s from 8 mM K_2PtCl_6 and 0.1 M HCl in the absence (**a**) or presence (**b**) of 0.05 mM $Pb(CH_3COO)_2$

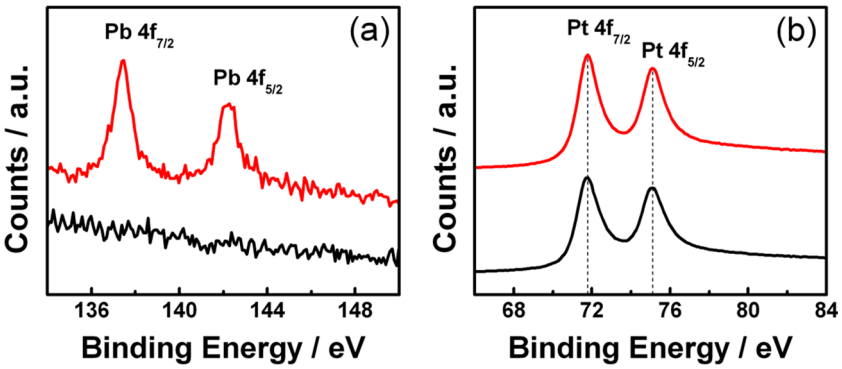

Fig. 3 XPS spectra for the Pb 4f region (**a**) and Pt 4f region (**b**) for nanostructured platinum electrodeposited in the absence (*black*) or presence (*red*) of $Pb(CH_3COO)_2$

In order to examine the surface chemistry of the electrodeposited materials, XPS studies were performed. As shown in Fig. 3a, no Pb could be detected for the quasi-spherical surfaces (black), whereas the spectrum recorded from the dendritic-like nanostructured materials (red) shows peaks at 137.4 and 142.3 eV, which are attributed to the Pb $4f_{7/2}$ and $4f_{5/2}$ core levels of PbO, respectively [59]. It should be noted, however, that the oxidation of Pb may have occurred after the removal of the sample from the electrodeposition solution as opposed to the direct electrochemical formation of PbO. While these peaks clearly indicate the presence of lead as lead oxide on the dendritic nanostructures, the intensity of these peaks is very low and suggests that the surface ratio of lead in the electrodeposited material is only 2.5 %. This low percentage is consistent with the cyclic voltammograms presented in Fig. 1, where it was seen that the bulk electrodeposition of platinum is the dominant process and that the accompanied lead UPD process on platinum is totally masked. In addition, a strong driving force exists for the galvanic replacement of electrodeposited Pb with Pt [60]. This reaction is likely to have occurred not only during the brief time between the end of the electrodeposition and cleaning the surface with Milli-Q water, but also during the electrodeposition reaction. In this manner, the surface of the growing electrodeposit is roughened and the formation of branched structures is promoted, while the surface concentration of Pb in the final deposit remains at a low level.

The crystallographic orientation of the platinum and platinum-lead surfaces was then probed by XRD (Fig. 4), and for clarity, the contribution from the underlying glassy carbon substrates was subtracted from the XRD patterns. As can be seen, the presence of lead does not cause any significant differences in these patterns, which was surprising given the noticeably altered morphology of the surfaces (Fig. 2). These results instead demonstrate that the lead changes the shape of the electrodeposit while maintaining a similar crystallographic structure. Both of these samples are polycrystalline, with a predominant (111) peak but with significant contributions from the (200) and (220) planes as well. The absence of peak shifts by the inclusion of lead in the material is consistent with previous studies on platinum and platinum-lead nanomaterials [61]. This was also reported for platinum-lead nanostructures with an estimated 41 % loading of lead [62], a value which is significantly higher than the lead surface coverage determined in this work (2.5 %).

The growth of the samples was further studied by conducting time dependent electrodeposition experiments (Fig. 5), with the electrodeposition terminated after 150 s (Fig. 5a, b), 300 s (Fig. 5c, d) and 600 s (Fig. 5e, f) for samples deposited in the absence (Fig. 5a, c, e) or presence (Fig. 5b, d, f) of lead acetate. For the platinum electrodeposited in the absence of lead acetate, a range of particle sizes can be observed after electrodeposition for 150 s (Fig. 5a), with typical particle sizes lying between 80 and 260 nm with an average size of 215 nm. While there is some degree of heterogeneity in these particle sizes, the majority of particles are ca. 200 nm in diameter. Increasing the electrodeposition time to 300 s (Fig. 5c) results in the growth of these particles to an average size of 250 nm. The growth of several particles in close proximity to each other can be seen to occur, resulting in the connection of these particles with time. These trends are again observed after electrodepositing for 600 s (Fig. 5e),

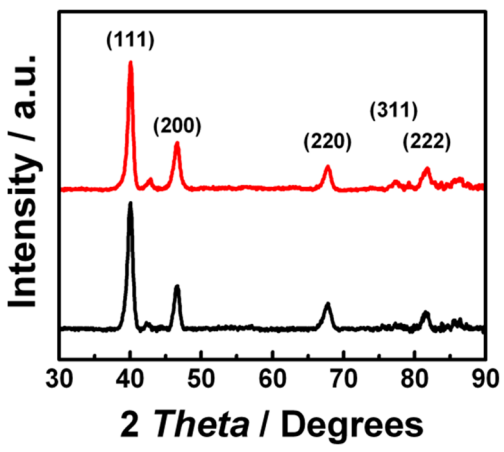

Fig. 4 XRD patterns for nanostructured platinum samples electrodeposited in the absence (*black*) or presence (*red*) of $Pb(CH_3COO)_2$. For clarity the patterns of the underlying GC substrate have been removed and the data normalised to the intensity of the (111) planes

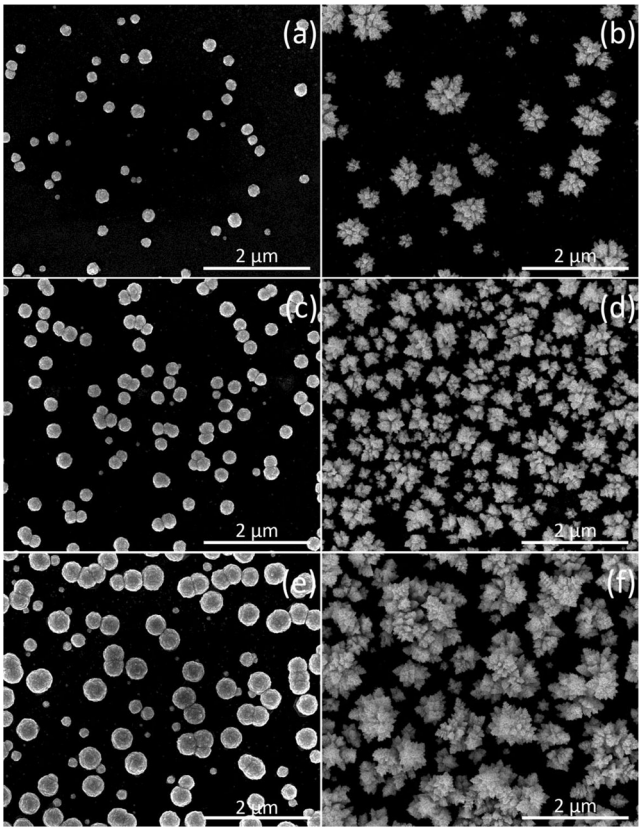

Fig. 5 SEM images of samples electrodeposited at −0.05 V from a solution containing 8 mM K_2PtCl_6 in 0.1 M HCl in the absence (**a**, **c**, **e**) or presence (**b**, **d**, **f**) of 0.05 mM $Pb(CH_3COO)_2$ for 150 s (**a**, **b**), 300 s (**c**, **d**) and 600 s (**e**, **f**)

where the typical particle size increases to an average size of 320 nm. Importantly, the morphology of the deposits is maintained across all times studied, suggesting that similar but smaller structures may be obtained at shorter time points.

Upon the introduction of lead acetate into the deposition solution, significant morphological changes can be observed, as demonstrated by the sample electrodeposited for 150 s (Fig. 5b). Here, a typical size of ca. 500 nm is observed, and a greater degree of size variation is seen at this sample than in the absence of lead acetate in the deposition solution, with particles as large as 900 nm present (the average size was determined to be 412 nm). When the electrodeposition is extended to 300 s (Fig. 5d), this size distribution is again evident, with particles ranging from approximately 80 to 500 nm in size, with an average size of 476 nm. A greater coverage of particles can also be seen across the sample when compared with the shorter electrodeposition time, which in addition to the range of particle sizes present suggests that the electrodeposition proceeds through a progressive nucleation process, where new nuclei are deposited whilst the existing particles continue to grow. This trend extends for the 600 s electrodeposition (Fig. 5f), with particles as small as 120 nm found alongside growths as large as 1.7 μm (an average size of 800 nm was determined). At all deposition times, larger particles are observed when lead acetate is included in the deposition solution, which is consistent with an increased rate of electrodeposition at −0.05 V in the presence of lead acetate. Also, of note is the formation of similar particle morphologies for all deposition times in the presence of lead acetate (Fig. 5b, d, f) as well as at a lower electrodeposition potential of −0.15 V (Fig. S2), indicating that the growth directing effect of the lead acetate can be maintained while controlling the size and coverage of the nanomaterials. This opens the possibility of electrodepositing similar dendritic nanostructures on a range of ubiquitous carbon nanomaterial supports such as carbon nanotubes, graphene and graphitic surfaces for use across a wide range of applications.

While glassy carbon provides a facile surface for the growth of platinum and platinum-lead materials, electrodeposition was also performed on indium tin oxide (ITO) films to investigate if the underlying electrode surface significantly influenced the morphology of the deposit and to establish if such nanostructures can be formed on other commonly employed support materials. As shown in Fig. 6 are the electrodeposition experiments performed in the absence

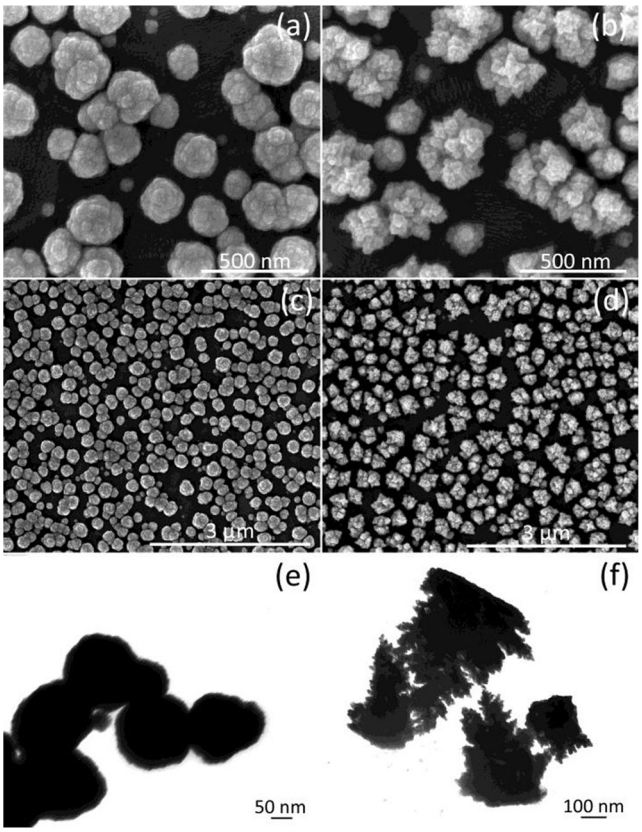

Fig. 6 SEM images of samples electrodeposited on indium tin oxide substrates at -0.05 V for 600 s from a solution of 8 mM K_2PtCl_6 in 0.1 M HCl in the absence (**a**, **c**) or presence (**b**, **d**) of 0.05 mM $Pb(CH_3COO)_2$. TEM images of these samples after sonication from the ITO surface are shown in (**e**) and (**f**) for samples deposited in the absence or presence of $Pb(CH_3COO)_2$, respectively

(Fig. 6a, c) or presence of 0.05 mM $Pb(CH_3COO)_2$ (Fig. 6b, d) on ITO. In the former case, platinum can be observed to form quasi-spherical shapes similar to those synthesised on glassy carbon; however, the particles display a more bush-like growth, with some formation of secondary particles visible on the initial deposits. The inclusion of lead acetate in the deposition solution causes the growth of isolated dendritic structures, also similar to those observed on glassy carbon substrates (Fig. 2). It can be seen from Fig. 6a and b as well as the lower magnification images in Fig. 6c and d that the electrodeposited materials cover the surface at a relatively high density, and unlike in the case of electrodeposition on glassy carbon the nanostructures are of similar sizes regardless of the presence of lead acetate. This is attributed to altered growth processes at the underlying ITO substrate compared with the glassy carbon substrates studied previously, as demonstrated by the cyclic voltammograms of ITO and glassy carbon in 8 mM K_2PtCl_6 in 0.1 M HCl (Fig. S3). The morphologies of the electrodeposited platinum and platinum-lead samples were also investigated by TEM imaging (Fig. 6e and f, respectively) after they were removed from the ITO surface by sonication. The quasi-spherical nature of the platinum materials is again observed (Fig. 6e), with a fine texture visible on the outer section of the particles and the growth of smaller nodules on the larger particles. The platinum-lead surface was however confirmed to be dendritic in nature, forming a large number of branches which in turn consist of fine tips (Fig. 6f). The similarity between these materials and the samples electrodeposited on glassy carbon illustrates that this dendritic growth is not the result of the underlying substrate, but is rather the direct influence of lead acetate on the growing electrodeposit. This adds further support that the underpotential deposition of lead on platinum (Fig. 1b) increases the formation of branched structures by disrupting the platinum surface during deposition, as well as indicating that such an approach may find broader application than for carbon-based materials alone. It has been reported that dendritic growth can be regarded as a competition between the order associated with crystal symmetry, as is the case for the deposition of Pt only, and instabilities that are induced in the system such as the presence of foreign species [63]. In this case, Pb as the foreign species which is deposited via a UPD process is competing with Pt deposition and therefore perturbs its growth. This is consistent with the theory for the co-crystallisation of metals where the presence of pinning centres, which are considered to be the metal at the lower concentration, induces disorder and result in the growth of side branches and ultimately dendrites [63].

Electrochemical behaviour of the nanostructured materials

The electrochemical behaviour of the electrodeposited materials was then examined in 1 M H_2SO_4, with the cyclic voltammograms of platinum electrodeposited on glassy carbon in the absence of lead acetate for 150 s (green), 300 s (blue) and 600 s (red) as well as a platinum electrode (black) shown in Fig. 7a. These scans originate at −0.25 V, which is just within the hydrogen evolution region, and upon the forward scan the reoxidation of hydrogen is observed at ca. −0.22 V. The desorption of hydrogen from the platinum surface can then be seen, with a broad oxidation peak at −0.06 V, after which no processes were observed within the double layer region prior to the onset of the monolayer oxide formation at ca. 0.73 V. On the reverse scan, this monolayer oxide is then reduced, with a peak potential of 0.48 V. Following this hydrogen adsorption is observed below ca. 0.08 V, before the onset of hydrogen evolution at ca. −0.18 V. The electrochemically active surface areas of the electrodeposited materials were calculated from the charge associated with the adsorption of hydrogen in this region. These calculations, based on a value of 210 μC cm^2 [64], indicate that the surface areas of the materials increase from 0.27 cm^2 for deposition at 150 s to 0.58 cm^2 at 300 s and finally 0.71 cm^2 at 600 s.

The voltammetric behaviour of the samples electrodeposited in the presence of lead acetate was also investigated, with the samples electrodeposited for 150 s (green), 300 s (blue) and 600 s (red) along with a polycrystalline platinum electrode (black) shown in Fig. 7b. These results show clear differences from the voltammograms in Fig. 7a, particularly in the

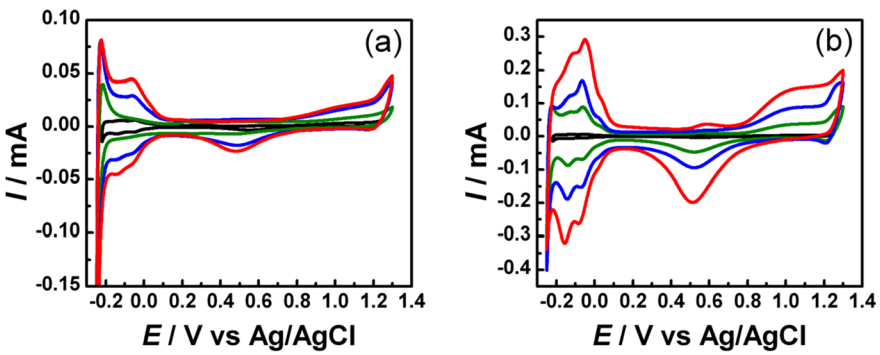

Fig. 7 Cyclic voltammograms recorded at 100 mV s in 1 M H_2SO_4 at a platinum electrode (*black*) and Pt nanostructures electrodeposited at −0.05 V for 150 s (*green*), 300 s (*blue*) and 600 s (*red*) in the absence (**a**) or presence (**b**) of 0.05 mM $Pb(CH_3COO)_2$

hydrogen region. The oxidation of the hydrogen reduced at the initial potential of −0.25 V can be seen at −0.21 V with desorption of hydrogen seen by peaks at −0.12 and −0.05 V and an inflection at 0.04 V. While the double layer region was found to be absent of peaks for the platinum electrodeposited without lead, in this case a peak can be observed with an onset potential of 0.47 V and a peak potential of 0.59 V. This peak is attributed to the premonolayer oxidation of platinum, showing a shift in onset potential of approximately 260 mV to lower potentials when compared with the onset of the monolayer oxide formation at ca. 0.73 V. Such premonolayer oxidation has previously been observed on platinum surfaces activated by polarisation in the hydrogen evolution region [6, 40, 41] or by severe thermal pretreatment followed by rapid quenching [36, 37] and has been attributed to the facile oxidation of low lattice coordinated surface atoms. On the reverse scan, the monolayer oxide is reduced in a broad process with a peak potential of 0.51 V, with the adsorption of hydrogen beginning at 0.11 V and marked by an inflection at 0.02 V and peaks at -0.08 and -0.16 V prior to the onset of hydrogen evolution at −0.22 V. The adsorption and desorption of hydrogen show much sharper peaks than the sample electrodeposited without the presence of lead acetate in the solution, indicating that the surface is more active towards these processes than the relatively sluggish processes occurring in Fig. 7a. Previous studies have been undertaken at single crystal electrodes in this region, which attribute the peaks at lower potential to the adsorption and desorption of hydrogen from the Pt (110) planes, while the peaks at a slightly more positive potential are related to the Pt (100) planes and a broad background current throughout this region attributed to processes on the Pt (111) surface [65]. While the determination of the relative proportion of the exposed crystal planes of polycrystalline platinum has previously been performed based on the adsorption of hydrogen, the analysis was complicated by the overlap of peaks from different single crystal electrodes and required additional information in the form of the oxidation of irreversibly adsorbed germanium [66]. Due to the complications involved in studying the electrodeposited platinum and platinum-lead nanostructures made here such a determination was not performed in this work.

The possibility that the peak at 0.59 V (Fig. 7b) is due to the oxidation of Pb_{UPD} formed during the synthesis needs to be considered. Previous work has shown that Pb is oxidatively desorbed in this potential region for studies where a lead salt is introduced into an acidic electrolyte at concentrations between 0.2 and 2 mM [56, 67]. In those studies, however, the deposition of lead not only resulted in a peak at a potential prior to monolayer oxide formation, but also resulted in a significant suppression of the hydrogen adsorption/desorption response where the peaks associated with strongly and weakly adsorbed hydrogen were no longer evident and a featureless region was observed. Further evidence to support that the oxidation peak observed here is not due to the oxidation of Pb_{UPD} is shown in Figure S4. This data shows the cyclic voltammetric behaviour of Pt which was electrodeposited from an electrolyte using double the lead acetate concentration of 1 mM while maintaining the concentration of K_2PtCl_6 at 8 mM. Although a higher surface area material is produced, as evidenced by the increase in area of the hydrogen adsorption/desorption region, the magnitude of the response at 0.59 V in relation to the increase in surface area does not change suggesting that this process is not associated with Pb_{UPD} oxidation as double the concentration of lead acetate was used.

The electrochemically active surface areas of the platinum-lead samples were also calculated from the adsorption of hydrogen, as discussed previously. The surface area was found to increase from 1.03 cm^2 after electrodeposition for 150 s to 2.25 cm^2 at 300 s and finally 3.15 cm^2 at 600 s. These values are significantly larger than the samples electrodeposited without lead acetate, with the largest surface area for these latter samples of 0.71 cm^2 at 600 s. Such results are consistent with the SEM images presented in Fig. 5, with the highly branched platinum-lead samples indicating a greater surface area than the quasi-spherical structures formed in the absence of lead acetate.

After investigating the active site behaviour of the electrodeposited nanomaterials in 1 M H_2SO_4, their electrocatalytic activity towards methanol oxidation in 1 M H_2SO_4 was then investigated. Illustrated in Fig. 8a is the response of a polycrystalline platinum electrode (black) and platinum electrodeposited in the absence of lead acetate for 150 s (green), 300 s (blue) and 600 s (red) in 1 M H_2SO_4 with 1 M methanol. As was discussed previously, increased electrodeposition times lead to increases in the electrochemically active surface areas of the materials, and so the methanol oxidation data has been normalised for the electrochemically active surface areas so that the specific activities of the materials may be compared. These scans were initiated at 0 V, where small features relating to the adsorption and desorption of hydrogen from the surfaces are observed. The forward scans then continue until an onset potential for methanol oxidation is observed at approximately 0.47 V, reaching a peak potential at ca. 0.69 V. A decrease in the rate of methanol oxidation is observed at potentials positive of this peak, as the formation of the monolayer oxide limits the sites available for methanol oxidation. Once this oxide is reduced on the reverse scan a peak appears at ca. 0.53 V, which has been reported as the oxidation of organic species formed in the forward scan such as CO_{ads}. However, this process has been readdressed, and it was found that the peak currents in both the forward and reverse scans were in fact related to the oxidation of methanol [68]. The specific activity of the commercially available platinum electrode (black) is almost identical to the activity of platinum electrodeposited for 150 s, with peak values of 17.8 and 18.7 μA cm^{-2}, respectively. However, this activity increases

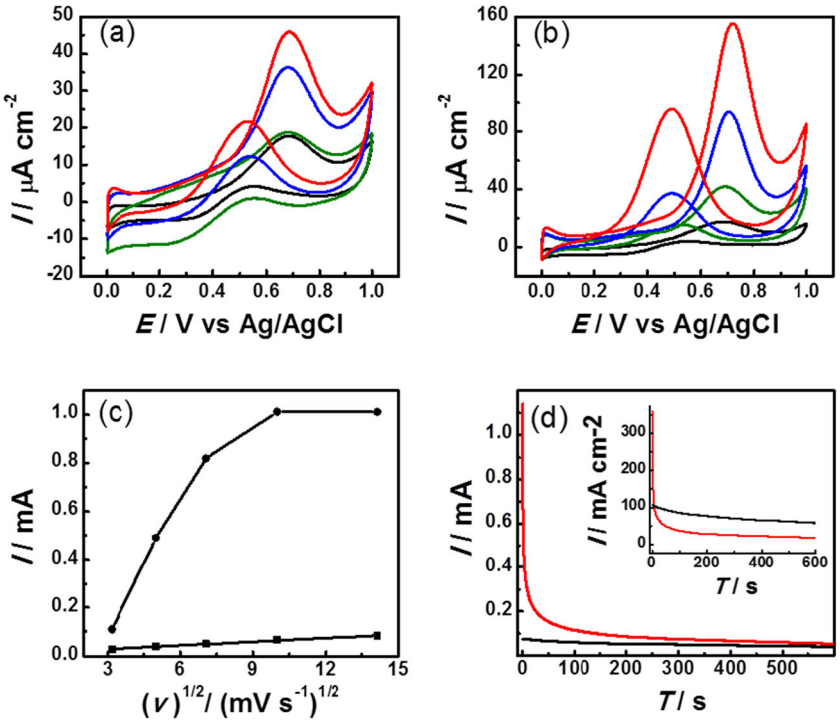

Fig. 8 CVs recorded in 1 M methanol in 1 M H_2SO_4 at a sweep rate of 50 mV s for a platinum electrode (*black*) and platinum nanostructures electrodeposited at −0.05 V for 150 s (*green*), 300 s (*blue*) and 600 s (*red*) in the absence (**a**) or presence (**b**) of 0.05 mM $Pb(CH_3COO)_2$, **c** plot of peak current versus $\nu^{1/2}$ for methanol oxidation at Pt electrodeposited in absence (*black square*) and presence of 0.05 mM $Pb(CH_3COO)_2$ (*red circle*), (**d**) chronoamperometry data recorded at 0.70 V for Pt electrodeposited in the absence (*black*) and presence (*red*) of 0.05 mM $Pb(CH_3COO)_2$ (inset shows the normalised data for surface area)

rapidly at samples electrodeposited for 300 and 600 s, with peak current densities of 36.3 and 45.8 μA cm^{-2}, respectively. The electrocatalytic oxidation of methanol was also investigated at the platinum-lead surfaces, as shown in Fig. 8b. Here, a clear difference exists between the specific activity of the commercial platinum electrode (black) and the sample electrodeposited for 150 s (green), increasing from 17.8 to 41.9 μA cm^{-2}, respectively. Further increases are then seen for longer electrodeposition times, with the 300 s sample (blue) showing an activity of 93.7 μA cm^2 and the 600 s sample (red) with a peak activity of 155.4 μA cm^{-2}. This latter value is more than three times the specific activity of the platinum sample electrodeposited for the same duration in the absence of lead acetate, showing that the inclusion of lead acetate during the electrodeposition creates a substantially more active electrocatalyst for methanol oxidation. These findings are also mirrored by the results obtained for platinum nanostructures electrodeposited on ITO (Fig. S5) showing that the increased surface area and electrocatalytic activity of the materials electrodeposited in the presence of lead acetate is linked to the deposition protocol rather than the underlying substrate.

The effect of sweep rate on methanol oxidation was also studied, and the cyclic voltammograms are shown in Fig. S6. For the case of the spherical Pt particles, there exists a clear linear relationship (R^2=0.98) between the peak current recorded on the positive sweep and square root of scan rate (Fig. 7c) which indicates a diffusion controlled process [69]. However, in the case of the PtPb material, this relationship does not hold. There is also not a linear dependence on scan rate which would have indicated a surface confined process. The peak position for Pt and PtPb materials shifts by 40 and 30 mV respectively upon a 20 fold increase in sweep rate and may be due to uncompensated resistance. Therefore, the mechanism of methanol oxidation at PtPb is more complicated and requires further investigation. However, it indicates that the reaction rate is not simply governed by the diffusion of methanol to the surface. There has been significant discussion on the methanol oxidation reaction at Pt surfaces which occurs via several steps [70]. Interestingly, Liu et al. proposed that active Pt atoms and $PtOH_{ads}$ species are responsible for the catalytic oxidation of methanol at premonolayer oxide potentials that is consistent with the IHOAM model [71].

It is known that PtPb bimetallic materials can possess enhanced electrocatalytic activity towards the oxidation of small organic molecules such as methanol [72–75], ethanol [76], formic acid [61, 75, 77–79] and glucose [80, 81] when compared to their monometallic Pt counterparts. The reasons for such improved electrocatalytic activity can include bifunctional effects [76, 77], whereby the added metal can enhance the activity by mitigating the poisoning of the active platinum surface by carbonaceous species such as CO_{ads}, electronic effects [74, 82, 83] where the electronic density of the platinum is altered by the presence of neighbouring Pb adatoms and geometric effects [72, 82, 84], where the formation of poisoning species is less favourable as their preferred binding sites become altered or blocked. It has also been noted that PbO_x nanomaterials can show electrocatalytic activity towards the reduction of oxygen [85] or the oxidation of formic acid [86] and ethanol [87], providing another possible means

for enhanced electrocatalysis on bimetallic PtPb nanomaterials. In the present case, the XPS and XRD data (Figs. 3 and 4, respectively) suggests that the electronic and crystallographic structures of the platinum are not significantly perturbed by the presence of Pb, making these unlikely causes for the improved methanol electrooxidation. Although we cannot rule out the bifunctional mechanism or the extent that the PbO_x influences the reaction, the surface coverage of Pb is much lower than in previously reported PtPb nanomaterials so these explanations are unlikely to fully account for the enhanced electrocatalytic activity. From the evidence presented, it is instead the altered morphology of the materials, with the sharp tips and fine features on the platinum-lead surfaces which increases the number of active sites available to promote the electrocatalytic oxidation of methanol, in agreement with the IHOAM model of electrocatalysis [6, 35, 36, 45, 71, 88, 89]. Increasing the mass activity of Pt by reducing the particle size is a further possibility which could be achieved by shortening the deposition time (dendrites are clearly formed at the shortest deposition time of 150 s) or by using a pulsed deposition protocol and will be the investigated in the future.

However, an interesting observation was found when the stability of the Pt and PtPb materials was investigated using chronoamperometry. The data in Fig. 7d shows that the PtPb materials show enhanced current at shorter times but the decay in current is quite rapid. The increased current over the time scale of the experiment recorded for the PtPb materials can be attributed to its increased surface area compared to Pt. When the data is normalised for the electrochemically active surface area (inset in Fig. 7d) then at shorter times enhanced current at PtPb compared to Pt is observed but this does not last and the specific activity decays below that observed for the spherical Pt particles. This result was unexpected given the promising voltammetry data in Fig. 7b and indicates that the oxidation of methanol at PtPb materials is prone to deactivation. Our previous study on gold electrocatalysis for the oxidation of methanol and hydrogen peroxide indicated that over oxidation of an active surface and extensive surface adsorption of OH^- ions resulted in poorer electrocatalytic activity [48]. Indeed, Burke has shown that a thermally activated Pt wire electrode that showed significant premonolayer oxide responses in acidic electrolyte demonstrated suppressed electrocatalytic activity for certain reactions and was related to over oxidation of active sites [36]. In that study, methanol oxidation was investigated that initially showed enhanced performance but decayed with time in quite a rapid manner when the electrode was activated by both thermal and electrochemical methods. It was pointed out that sustained methanol oxidation could be achieved at activated electrodes but was highly dependent on the activation conditions. Therefore, it appears in this study that the fabrication of dendritic materials with fine tips shows short-term enhanced performance but that the active sites may be prone to over oxidation that competes with methanol oxidation.

SERS activity of the electrodeposited nanostructures

The development of effective platinum-based surfaces for SERS applications is relevant since platinum is generally considered a poor material for SERS, with its surface plasmon absorption band lying outside the visible region. However, highly nanostructured materials can lead to more effective SERS materials through a number of effects such as the lightning rod effect and the presence of hot spots located between adjacent metallic structures. In light of the large number of fine features present on the nanostructured platinum-lead samples, these materials were therefore investigated for their application as SERS platforms. After immobilising Rhodamine B on the surface and removing any loosely adhered dye by rinsing the sample in Milli-Q water, the SERS spectrum presented in Fig. 9b was obtained for a platinum-lead nanomaterial electrodeposited for 600 s at −0.05 V, as shown by the side-on SEM image in Fig. 9a. Here, it can be seen that peaks due to Rhodamine B can be observed at 1,118; 1,198; 1,342; 1,464; 1,502; 1,584 and 1,630 cm^{-1}. It should be noted that no peaks were recorded for the quasi-spherical platinum nanostructures or for a planar platinum surface (data not shown), illustrating that the hierarchical platinum-lead nanostructures formed in this work present a viable method of creating SERS active platinum materials.

In order to further increase this SERS activity, the electrodeposition procedure was modified to increase the density of

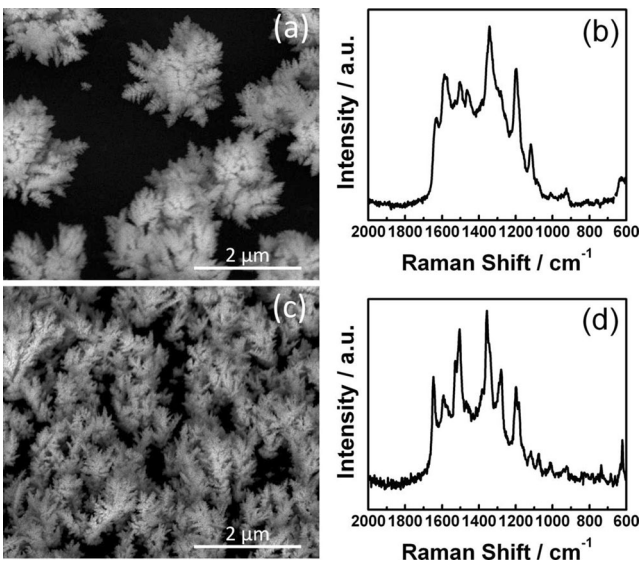

Fig. 9 SEM images recorded at an angle of 45° (**a** and **c**) and their corresponding SERS spectra (**b** and **d**) after Rhodamine B immobilisation on samples electrodeposited from a solution of 8 mM K_2PtCl_6 with 0.1 M HCl and 0.05 mM $Pb(CH_3COO)_2$, with the electrodeposition carried out for 600 s at a potential of −0.05 V (**a**, **b**) or −0.3 V (**c**, **d**)

the nanostructured features on the surface. This involved forming platinum-lead nanomaterials by electrodepositing for 600 s at -0.3 V, a potential which is within the hydrogen evolution region and is slightly lower than the range covered by the cyclic voltammogram in Fig. 1a. As seen from the SEM image recorded at 45° in Fig. 9c, this produced similar dendritic structures to those observed in Fig. 9a, although the deposits were smaller and an increased density of deposits was observed. While the formation of nanostructures with sharp tips is one method of creating SERS active substrates, the formation of nanosized junctions between metallic features has also been shown as a powerful means of creating SERS hotspots. In this case, the higher coverage of deposits on the surface facilitates the overlap of adjoining dendritic branches of the platinum-lead nanostructures, increasing the potential number of hotspots that are present. The SERS spectrum of Rhodamine B on this material (Fig. 9d) provides confirmation of this enhancement, with increased peak resolution observed compared with the sample electrodeposited at a higher potential (Fig. 9b). These results demonstrate that the platinum-lead nanomaterials formed by the electrodeposition of platinum in the presence of lead acetate are not only active materials for electrocatalysis but they are also promising materials for SERS applications, which may be of importance for the study of electro(catalytic) processes at platinum surfaces using this powerful spectroscopic technique.

Conclusions

The formation of platinum rich platinum-lead nanostructured materials with a large number of sharp tips was achieved through the electrochemical reduction of Pt^{4+} in the presence of lead acetate. The latter species acted as a growth directing agent for the electrodeposited material by perturbing the growth of Pt via a competing UPD process and inducing branched growth which ultimately led to dendritic structures. The UPD of Pb can be considered as a dynamic template which results in a low degree of incorporation of the secondary metal into the final material. Significantly, premonolayer oxidation takes place at active sites on the surface of the dendritic materials which also demonstrate enhanced performance for the oxidation of methanol compared to spherical Pt nanomaterials electrodeposited in the absence of lead acetate in the plating solution under cyclic voltammetry conditions. However, sustained methanol oxidation was prone to deactivation and may be related to over oxidation of active sites on the surface, indicating that the tuning of morphology and active site behaviour is critical to enhanced performance. Significantly, however, these hierarchical nanomaterials were found to be active SERS substrates, in contrast to the quasi-spherical Pt nanostructures formed in the absence of lead acetate in the electrolyte. The formation of dendritic platinum surfaces may prove significant as it provides a suitable nanomaterial to study chemical or electrochemical reactions occurring on platinum surfaces via the SERS technique whilst avoiding the presence of organic growth direction agents which could interfere with the obtained spectra. This highlights the multifunctional role of the platinum-lead nanomaterials formed through the templating effect of lead acetate and provides a facile route for the possible synthesis of a range of other nanostructured materials via initiating the UPD of a secondary metal during the course of electroreduction of the primary metal.

Acknowledgments The financial support from the Platform Technologies Research Institute, RMIT University (AOM) and the Australian Research Council through the Future Fellowship Scheme FT110100760 (AOM) and Discovery Project DP0988099 (AOM, VB, SKB) is gratefully acknowledged. The authors also acknowledge the facilities and the scientific and technical assistance of the Australian Microscopy and Microanalysis Research Facility at the RMIT Microscopy and Microanalysis Facility.

References

1. Heo J, Kim D-S, Kim ZH, Lee YW, Kim D, Kim M, Kwon K, Park HJ, Yun WS, Han SW (2008) Controlled synthesis and characterization of the enhanced local field of octahedral Au nanocrystals. Chem Commun 6120–6122
2. Tian N, Zhou Z-Y, Sun S-G, Cui L, Ren B, Tian Z-Q (2006) Electrochemical preparation of platinum nanothorn assemblies with high surface enhanced Raman scattering activity. Chem Commun 4090–4092
3. Zhang H, Xu J-J, Chen H-Y (2008) Shape-controlled gold nanoarchitectures: Synthesis, superhydrophobicity, and electrocatalytic properties. J Phys Chem C 112:13886–13892
4. Gimeno Y, Hernández Creus A, González S, Salvarezza RC, Arvia AJ (2001) Preparation of 100–160-nm-sized branched palladium islands with enhanced electrocatalytic properties on HOPG. Chem Mater 13:1857–1864
5. Abdelsalam ME, Mahajan S, Bartlett PN, Baumberg JJ, Russell AE (2007) SERS at structured palladium and platinum surfaces. J Am Chem Soc 129:7399–7406
6. Burke LD, Horgan MA, Hurley LM, Nagle LC, O'Mullane AP (2001) Superactivation of metal electrode surfaces and its relevance to CO_{ads} oxidation at fuel cell anodes. J Appl Electrochem 31:729–738
7. Chen Y-X, Chen S-P, Chen Q-S, Zhou Z-Y, Sun S-G (2008) Electrochemical preparation of iron cuboid nanoparticles and their catalytic properties for nitrite reduction. Electrochim Acta 53:6938–6943
8. Guo S, Dong S, Wang E (2008) A general method for the rapid synthesis of hollow metallic or bimetallic nanoelectrocatalysts with urchinlike morphology. Chem Eur J 14:4689–4695
9. Hutton L, Newton ME, Unwin PR, Macpherson JV (2008) Amperometric oxygen sensor based on a platinum nanoparticle-modified polycrystalline boron doped diamond disk electrode. Anal Chem 81:1023–1032
10. Lee EP, Peng Z, Chen W, Chen S, Yang H, Xia Y (2008) Electrocatalytic properties of Pt nanowires supported on Pt and W Gauzes. ACS Nano 2:2167–2173

11. O'Mullane AP, Dale SE, Macpherson JV, Unwin PR (2004) Fabrication and electrocatalytic properties of polyaniline/Pt nanoparticle composites. Chem Commun 1606–1607
12. Rhee CK, Kim B-J, Ham C, Kim Y-J, Song K, Kwon K (2009) Size effect of Pt nanoparticle on catalytic activity in oxidation of methanol and formic acid: Comparison to Pt(111), Pt(100), and polycrystalline Pt electrodes. Langmuir 25:7140–7147
13. Subhramannia M, Ramaiyan K, Pillai VK (2008) Comparative study of the shape-dependent electrocatalytic activity of platinum multipods, discs, and hexagons: Applications for fuel cells. Langmuir 24:3576–3583
14. Tiwari JN, Pan F-M, Tiwari RN, Nandi SK (2008) Facile synthesis of continuous Pt island networks and their electrochemical properties for methanol electrooxidation. Chem Commun 6516–6518
15. Tominaka S, Wu C-W, Momma T, Kuroda K, Osaka T (2008) Perpendicular mesoporous Pt thin films: Electrodeposition from titania nanopillars and their electrochemical properties. Chem Commun 2888–2890
16. Wang C, Daimon H, Onodera T, Koda T, Sun S (2008) A general approach to the size- and shape-controlled synthesis of platinum nanoparticles and their catalytic reduction of oxygen. Angew Chem Int Ed 47:3588–3591
17. Yang M, Yang Y, Liu Y, Shen G, Yu R (2006) Platinum nanoparticles-doped sol–gel/carbon nanotubes composite electrochemical sensors and biosensors. Biosens Bioelectron 21:1125–1131
18. Zhou Z-Y, Tian N, Huang Z-Z, Chen D-J, Sun S-G (2009) Nanoparticle catalysts with high energy surfaces and enhanced activity synthesized by electrochemical method. Faraday Discuss 140:81–92
19. Chen J, Herricks T, Xia Y (2005) Polyol synthesis of platinum nanostructures: Control of morphology through the manipulation of reduction kinetics. Angew Chem Int Ed 44:2589–2592
20. Herricks T, Chen J, Xia Y (2004) Polyol synthesis of platinum nanoparticles: Control of morphology with sodium nitrate. Nano Lett 4:2367–2371
21. Tsung C-K, Kuhn JN, Huang W, Aliaga C, Hung L-I, Somorjai GA, Yang P (2009) Sub-10 nm platinum nanocrystals with size and shape control: catalytic study for ethylene and pyrrole hydrogenation. J Am Chem Soc 131:5816–5822
22. Yang D, Sun S, Meng H, Dodelet J-P, Sacher E (2008) Formation of a porous platinum nanoparticle froth for electrochemical applications, produced without templates, surfactants, or stabilizers. Chem Mater 20:4677–4681
23. Tian N, Zhou Z-Y, Sun S-G, Ding Y, Wang ZL (2007) Synthesis of tetrahexahedral platinum nanocrystals with high-index facets and high electro-oxidation activity. Science 316:732–735
24. Tian N, Zhou Z-Y, Sun S-G (2008) Platinum metal catalysts of high-index surfaces: from single-crystal planes to electrochemically shape-controlled nanoparticles. J Phys Chem C 112:19801–19817
25. Awad MI, El-Deab MS, Ohsaka T (2007) Tailor-designed platinum nanoparticles electrodeposited onto gold electrode: Catalytic activity for oxygen reduction. J Electrochem Soc 154:B810–B816
26. Qian L, Liu Y, Song Y, Li Z, Yang X (2005) Electrodeposition of Pt nanoclusters on the surface modified by monolayer poly(amidoamine) dendrimer film. Electrochem Commun 7:1209–1212
27. Sun Y, Sun L, Xu F, Guo C, Liu Z, Zhang Y, Yang T, Li Z (2009) Electrodeposition of platinum nanoclusters on type I collagen modified electrode and its electrocatalytic activity for methanol oxidation. Appl Surf Sci 255:6814–6818
28. Ye F, Li J, Wang T, Liu Y, Wei H, Li J, Wang X (2008) Electrocatalytic properties of platinum catalysts prepared by pulse electrodeposition method using SnO_2 as an assisting reagent. J Phys Chem C 112:12894–12898
29. Attard GS, Bartlett PN, Coleman NRB, Elliott JM, Owen JR, Wang JH (1997) Mesoporous platinum films from lyotropic liquid crystalline phases. Science 278:838–840
30. Kijima T, Nagatomo Y, Takemoto H, Uota M, Fujikawa D, Sekiya Y, Kishishita T, Shimoda M, Yoshimura T, Kawasaki H, Sakai G (2009) Synthesis of nanohole-structured single-crystalline platinum nanosheets using surfactant-liquid-crystals and their electrochemical. Adv Funct Mater 19:545–553
31. Saitou M (2006) Electrochemical characterization of platinum black electrodeposited from electrolyte including lead acetate trihydrate. Surf Coat Technol 201:3611–3614
32. Ye F, Chen L, Li J, Li J, Wang X (2008) Shape-controlled fabrication of platinum electrocatalyst by pulse electrodeposition. Electrochem Commun 10:476–479
33. Das J, Patra S, Yang H (2008) Enhancement of the electrocatalytic activity of gold nanoparticles via $NaBH_4$ treatment. Chem Commun 4451–4453
34. Burke D, O'Mullane A, Lodge V, Mooney M (2001) Auto-inhibition of hydrogen gas evolution on gold in aqueous acid solution. J Solid State Electrochem 5:319–327
35. Burke LD (2004) Scope for new applications for gold arising from the electrocatalytic behaviour of its metastable surface states. Gold Bull 37:125–135
36. Burke LD, Hurley LM (1999) The redox behaviour of thermally pretreated, highly disrupted, states of platinum surfaces in aqueous media. Electrochim Acta 44:3451–3473
37. Burke LD, Hurley LM (2000) Redox behaviour of thermally activated platinum electrodes with particular reference to operation at elevated temperature. J Solid State Electrochem 4:353–362
38. Burke LD, Hurley LM, Lodge VE, Mooney MB (2001) The effect of severe thermal pretreatment on the redox behaviour of gold in aqueous acid solution. J Solid State Electrochem 5:250–260
39. Burke LD, O'Mullane AP (2000) Generation of active surface states of gold and the role of such states in electrocatalysis. J Solid State Electrochem 4:285–297
40. Díaz V, Real S, Téliz E, Zinola CF, Martins ME (2009) New experimental evidence on the formation of platinum superactive sites in an electrochemical environment. Int J Hydrog Energy 34:3519–3530
41. Díaz V, Zinola CF (2007) Catalytic effects on methanol oxidation produced by cathodization of platinum electrodes. J Colloid Inter Sci 313:232–247
42. Yanson AI, Rodriguez P, Garcia-Araez N, Mom RV, Tichelaar FD, Koper MTM (2011) Cathodic corrosion: a quick, clean, and versatile method for the synthesis of metallic nanoparticles. Angew Chem Int Ed 50:6346–6350
43. O'Mullane AP (2014) From single crystal surfaces to single atoms: Investigating active sites in electrocatalysis. Nanoscale 6:4012–4026
44. Kleijn SE, Lai SC, Koper MT, Unwin PR (2014) Electrochemistry of nanoparticles. Angew Chem Int Ed 53:3558–86
45. Burke L, Casey J, Morrissey J, Murphy M (1991) Incipient hydrous oxide/adatom mediator model of electrocatalysis. Bull Electrochem 7:506–511
46. Nowicka AM, Hasse U, Sievers G, Donten M, Stojek Z, Fletcher S, Scholz F (2010) Selective knockout of gold active sites. Angew Chem Int Ed 49:3006–3009
47. Nowicka AM, Hasse U, Donten M, Hermes M, Stojek ZJ, Scholz F (2011) The treatment of Ag, Pd, Au and Pt electrodes with OH• radicals reveals information on the nature of the electrocatalytic centers. J Solid State Electrochem 15:2141–2147
48. O'Mullane AP, Ippolito SJ, Sabri YM, Bansal V, Bhargava SK (2009) Premonolayer oxidation of nanostructured gold: an important factor influencing electrocatalytic activity. Langmuir 25:3845
49. Arvia A, Salvarezza R, Triaca W (2004) Noble metal surfaces and electrocatalysis. Review and perspectives. J New Mater Electrochem Syst 7:133–144
50. Gómez R, Pérez JM, Solla-Gullón J, Montiel V, Aldaz A (2004) In situ surface enhanced Raman spectroscopy on electrodes with platinum and palladium nanoparticle ensembles. J Phys Chem B 108: 9943–9949

51. Lee H-J, Lee UH, Park J-Y, Yoo S-H, Park S, Kwon Y-U (2009) Platinum films with controlled 3-dimensional nanoscopic morphologies and their effects on surface enhanced Raman scattering. Chem Asian J 4:1284–1288
52. Mrozek MF, Xie Y, Weaver MJ (2001) Surface-enhanced Raman scattering on uniform platinum-group overlayers: Preparation by redox replacement of underpotential-deposited metals on gold. Anal Chem 73:5953–5960
53. Park S, Yang P, Corredor P, Weaver MJ (2002) Transition metal-coated nanoparticle films: vibrational characterization with surface-enhanced Raman scattering. J Am Chem Soc 124:2428–2429
54. Kim K, Kim KL, Lee HB, Shin KS (2010) Surface-enhanced Raman scattering on aggregates of platinum nanoparticles with definite size. J Phys Chem C 114:18679–18685
55. Lu G, Zangari G (2005) Electrodeposition of platinum on highly oriented pyrolytic graphite. Part I: electrochemical characterization. J Phys Chem B 109:7998–8007
56. Wilde CP, Zhang M (1992) Adsorption and underpotential deposition of lead at electrodeposited platinum electrodes. J Electroanal Chem 327:307–320
57. Ott A, Jones LA, Bhargava SK (2011) Direct electrodeposition of porous platinum honeycomb structures. Electrochem Commun 13: 1248–1251
58. Mayrhofer KJJ, Blizanac BB, Arenz M, Stamenkovic VR, Ross PN, Markovic NM (2005) The impact of geometric and surface electronic properties of Pt-catalysts on the particle size effect in electrocatalysis. J Phys Chem B 109:14433–14440
59. Dai G, Xu J (1998) Low pressure chemical vapor deposition of PbO thin film from lead dichloride. J Mater Sc Lett 17:969–971
60. Van Brussel M, Kokkinidis G, Hubin A, Buess-Herman C (2003) Oxygen reduction at platinum modified gold electrodes. Electrochim Acta 48:3909–3919
61. Buzzo GS, Orlandi MJB, Teixeira-Neto E, Suffredini HB (2011) On the proportion of Pb and Pt in carbon-supported electrocatalysts. Int J Electrochem Sci 6:3768–3775
62. Chen D-J, Zhou Z-Y, Wang Q, Xiang D-M, Tian N, Sun S-G (2010) A non-intermetallic PtPb/C catalyst of hollow structure with high activity and stability for electrooxidation of formic acid. Chem Commun 46:4252–4254
63. Wang J, Asmussen RM, Adams B, Thomas DF, Chen A (2009) Facile synthesis and electrochemical properties of intermetallic PtPb nanodendrites. Chem Mater 21:1716–1724
64. Wang J, Swain GM (2003) Fabrication and evaluation of platinum/diamond composite electrodes for electrocatalysis: preliminary studies of the oxygen-reduction reaction. J Electrochem Soc 150:E24–E32
65. Jambunathan K, Shah BC, Hudson JL, Hillier AC (2001) Scanning electrochemical microscopy of hydrogen electro-oxidation. Rate constant measurements and carbon monoxide poisoning on platinum. J Electroanal Chem 500:279–289
66. Solla-Gullon J, Rodriguez P, Herrero E, Aldaz A, Feliu JM (2008) Surface characterization of platinum electrodes. Phys Chem Chem Phys 10:1359–1373
67. Machado SAS, Tanaka AA, Gonzalez ER (1994) Underpotential deposition of lead on polycrystalline platinum and its influence on the oxygen reduction reaction. Electrochim Acta 39:2591–2597
68. Hofstead-Duffy AM, Chen D-J, Sun S-G, Tong YJ (2012) Origin of the current peak of negative scan in the cyclic voltammetry of methanol electro-oxidation on Pt-based electrocatalysts: a revisit to the current ratio criterion. J Mater Chem 22:5205–5208
69. He Z, Chen J, Liu D, Tang H, Deng W, Kuang Y (2004) Deposition and electrocatalytic properties of platinum nanoparticals on carbon nanotubes for methanol electrooxidation. Mater Chem Phys 85:396–401
70. Iwasita T (2002) Electrocatalysis of methanol oxidation. Electrochim Acta 47:3663–3674
71. Hu C-C, Liu K-Y (1999) Voltammetric investigation of platinum oxides. I. Effects of ageing on their formation/reduction behavior as well as catalytic activities for methanol oxidation. Electrochim Acta 44:2727–2738
72. Casado-Rivera E, Volpe DJ, Alden L, Lind C, Downie C, Vázquez-Alvarez T, Angelo ACD, DiSalvo FJ, Abruña HD (2004) Electrocatalytic activity of ordered intermetallic phases for fuel cell applications. J Am Chem Soc 126:4043–4049
73. Beden B, Kadirgan F, Lamy C, Leger JM (1981) Electrocatalytic oxidation of methanol on platinum-based binary electrodes. J Electroanal Chem 127:75–85
74. Jiang Q, Jiang L, Qi J, Wang S, Sun G (2011) Experimental and density functional theory studies on PtPb/C bimetallic electrocatalysts for methanol electrooxidation reaction in alkaline media. Electrochim Acta 56:6431–6440
75. Huang Y, Zheng S, Lin X, Su L, Guo Y (2012) Microwave synthesis and electrochemical performance of a PtPb alloy catalyst for methanol and formic acid oxidation. Electrochim Acta 63:346–353
76. Huang Y, Cai J, Liu M, Guo Y (2012) Fabrication of a novel PtPbBi/C catalyst for ethanol electro-oxidation in alkaline medium. Electrochim Acta 83:1–6
77. Lei H-W, Hattori H, Kita H (1996) Electrocatalysis by Pb adatoms of HCOOH oxidation at Pt(111) in acidic solution. Electrochim Acta 41: 1619–1628
78. Hwang S-M, Bonevich JE, Kim JJ, Moffat TP (2011) Formic acid oxidation on $Pt_{100-x}Pb_x$ thin films electrodeposited on Au. J Electrochem Soc 158:B1019–B1028
79. Yu X, Pickup PG (2010) Pb and Sb modified Pt/C catalysts for direct formic acid fuel cells. Electrochim Acta 55:7354–7361
80. Wang J, Thomas DF, Chen A (2008) Nonenzymatic electrochemical glucose sensor based on nanoporous PtPb networks. Anal Chem 80: 997–1004
81. Cui HF, Ye JS, Zhang WD, Li CM, Luong JH, Sheu FS (2007) Selective and sensitive electrochemical detection of glucose in neutral solution using platinum-lead alloy nanoparticle/carbon nanotube nanocomposites. Anal Chim Acta 594:175–83
82. Zhang LJ, Wang ZY, Xia DG (2006) Bimetallic PtPb for formic acid electro-oxidation. J Alloys Compd 426:268–271
83. Papadimitriou S, Tegou A, Pavlidou E, Kokkinidis G, Sotiropoulos S (2007) Methanol oxidation at platinized lead coatings prepared by a two-step electrodeposition–electroless deposition process on glassy carbon and platinum substrates. Electrochim Acta 52:6254–6260
84. Pletcher D (1984) Electrocatalysis: Present and future. J Appl Electrochem 14:403–415
85. Wang Y, Laborda E, Plowman BJ, Tschulik K, Ward KR, Palgrave RG, Damm C, Compton RG (2014) The strong catalytic effect of Pb(II) on the oxygen reduction reaction on 5 nm gold nanoparticles. Phys Chem Chem Phys 16:3200–3208
86. Buzzo GS, Niquirilo RV, Suffredini HB (2010) Active Pt-PbO_x:C Anodes to promote the formic acid oxidation in presence of sulfuric acid. J Braz Chem Soc 21:185–190
87. Yang WH, Wang HH, Chen DH, Zhou ZY, Sun SG (2012) Facile synthesis of a platinum-lead oxide nanocomposite catalyst with high activity and durability for ethanol electrooxidation. Phys Chem Chem Phys 14:16424–32
88. Collins JA, The IHOAM model of electrocatalysis: with particular reference to copper. 1999: NUI, 1999 at Department of Chemistry, UCC.
89. Lertanantawong B, O'Mullane AP, Surareungchai W, Somasundrum M, Burke LD, Bond AM (2008) Study of the underlying electrochemistry of polycrystalline gold electrodes in aqueous solution and electrocatalysis by large amplitude Fourier transformed alternating current voltammetry. Langmuir 24:2856–2868